ACS Macro Letters

pubs.acs.org/macroletters Letter

Microfluidic Fabrication of Phase-Inverted Microcapsules with Asymmetric Shell Membranes with Graded Porosity

Zhang Wu, Jörg G. Werner,* and David A. Weitz*

Cite This: ACS Macro Lett. 2021, 10, 116−121 Read Online

ACCESS | Metrics & More | Article Recommendations | Supporting Information

ABSTRACT: Microcapsules with liquid cores and solid shells are attractive as dispersible protective micron-sized containers. Applications that rely on molecular mass transport often require a combination of size selectivity, high permeability, and mechanical stability. Capsule architectures that combine all these features represent a material property, design, and fabrication challenge. In this work, the design of an asymmetric microcapsule shell architecture is reported to achieve a good combination of the desired features. Poly(methyl methacrylate) phase-inverted microcapsules featuring an asymmetric graded macroporous shell covered with a dense skin separation layer are obtained from water-in-oil-in-water double emulsion drops that are phase-inverted in a water-based coagulation bath. The phase-inverted microcapsules exhibit good mechanical stability and allow for high permeability of its shell membrane with molecular size dependence.

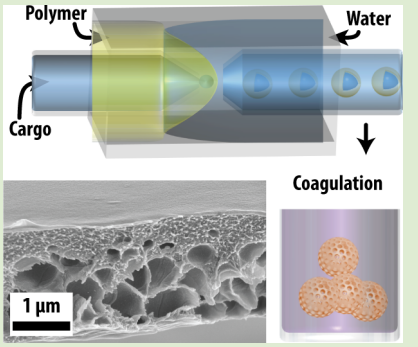

Microcapsules with functional shells are important potential candidates for dispersed microreactors, carriers, and sensors.[1−6] This requires the shell structures to be designed with tailored mechanical properties and to provide a protective layer for the encapsulated cargo as well as an interface for interaction between encapsulants and the environment.[7−11] For example, semipermeable microcapsules whose membranes allow the transport of small molecules while rejecting larger macromolecules and particulate matter will ensure selective exchange of signals and nutrients across the capsule shells,[12−15] and thereby be useful for cell encapsulation in immunoisolation.[16−18] The shells protect the cells from exposure to the innate immune system of human.[19] Under some cases, however, the capsules may not resist the substantial environmental mechanical stresses arising from osmolarity change or external mechanical forces, thus undergoing mechanical impairment or even breakdown. To optimize the selective transmembrane mass transport as well as ensure that the capsules stay robustly intact in delivery as protective carriers, selective and permeable capsule membranes with mechanical stability are required. However, a good combination of all these three features is not easy to achieve. To increase permeability yet retain size-selective control, selective layers of membranes with a decreasing thickness or increasing open pores are commonly adopted. But reducing the thickness compromises structural stability, while raising the porosity of the selective layers compromises the selectivity resolution. Although higher structural stability can be achieved by making the membranes thicker, it impedes high permeability. Therefore, well-designed architectures need to be developed for capsule membranes to achieve a good combination of the selectivity resolution, permeability, and mechanical properties. This is essential to ensure microcapsules with functional shells achieve their full potential.

Here, we report the fabrication of selective, permeable, and mechanically stable capsule membranes. A composite asymmetric membrane architecture integrating an ultrathin size-selective separation layer and a second highly porous supportive sublayer is introduced in capsule shells. Double-emulsion templating is adopted to generate capsules, and a phase inversion technique is utilized to induce phase separation within the capsule shells to form the asymmetric structure. Water-in-oil-in-water (W/O/W) double emulsion drops are fabricated in microfluidic drop makers. The oil shell contains poly(methyl methacrylate) (PMMA) polymer, which is subsequently precipitated in a coagulation bath with a mixture of dimethyl sulfoxide (DMSO) and water. The process yields asymmetric microcapsule shells that possess an ultrathin separation layer on top of a graded macroporous sublayer. The microcapsules with the asymmetric shell structure exhibit high permeability for small dye molecules and are size-selective for molecules with different molecular weights. Moreover, the asymmetric microcapsules demonstrate good structural integrity during both fabrication and the permeation test.

A glass capillary microfluidic device is adopted for the fabrication of homogeneous W/O/W double emulsion droplets to template the water-cored microcapsules.[20−22] The

Received: December 14, 2020
Accepted: December 24, 2020

https://dx.doi.org/10.1021/acsmacrolett.0c00858
ACS Macro Lett. 2021, 10, 116−121

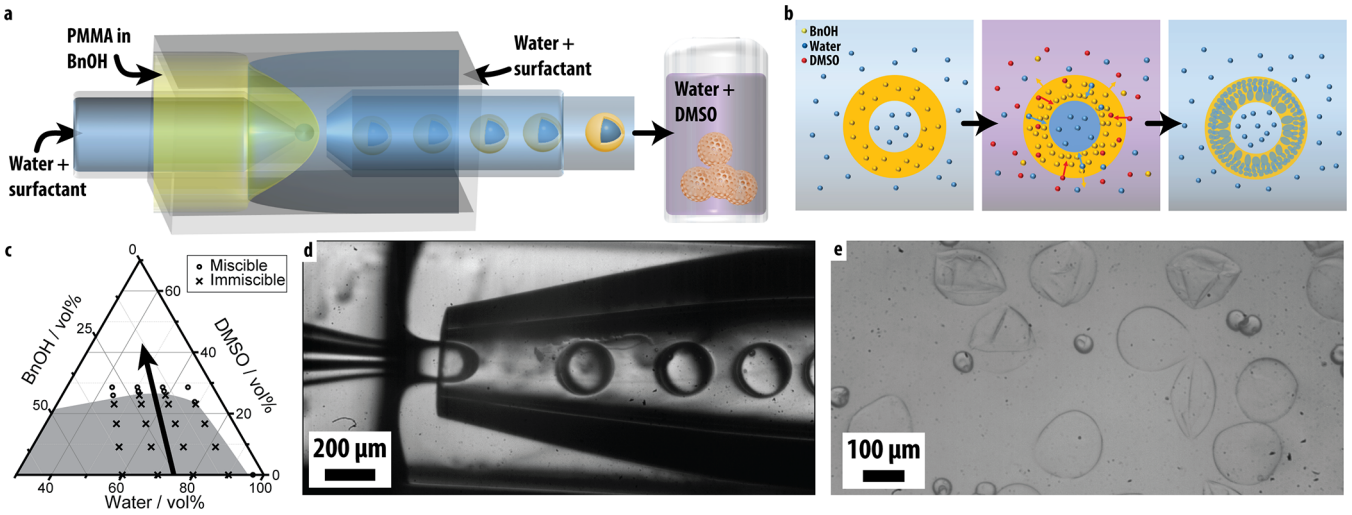

Figure 1. (a, b) Illustration of double emulsion drop fabrication and subsequent non-solvent-induced phase separation (NIPS). (a) Water-in-benzyl alcohol-in-water double emulsion drops with PMMA dissolved in the benzyl alcohol phase are fabricated in a glass capillary microfluidic drop maker and collected in a coagulation bath of water and DMSO that induces phase inversion in the shell. (b) The NIPS process with a double emulsion drop: The benzyl alcohol solution of PMMA in the shell phase is immiscible with the inner and outer aqueous phases, yielding emulsion drops (left) that undergo phase inversion in the water−DMSO coagulation mixture, where the benzyl alcohol diffuses from the shell into the surrounding medium, and water and DMSO diffuse into the PMMA-containing benzyl alcohol shell (middle), inducing phase separation and solidification of the PMMA, yielding a porous PMMA shell (right). (c) Experimental three-component phase diagram of water, benzyl alcohol, and DMSO. Crosses and circles indicate immiscible and miscible compositions, respectively. The gray area indicates the two-phase region; the white area indicates the one-phase region. The arrow indicates the change in composition during NIPS. (d, e) Optical microscopy image of the double emulsion drop formation in a glass capillary microfluidic drop maker (d) and of PMMA microcapsules immediately after phase inversion in a water/DMSO coagulation bath (e).

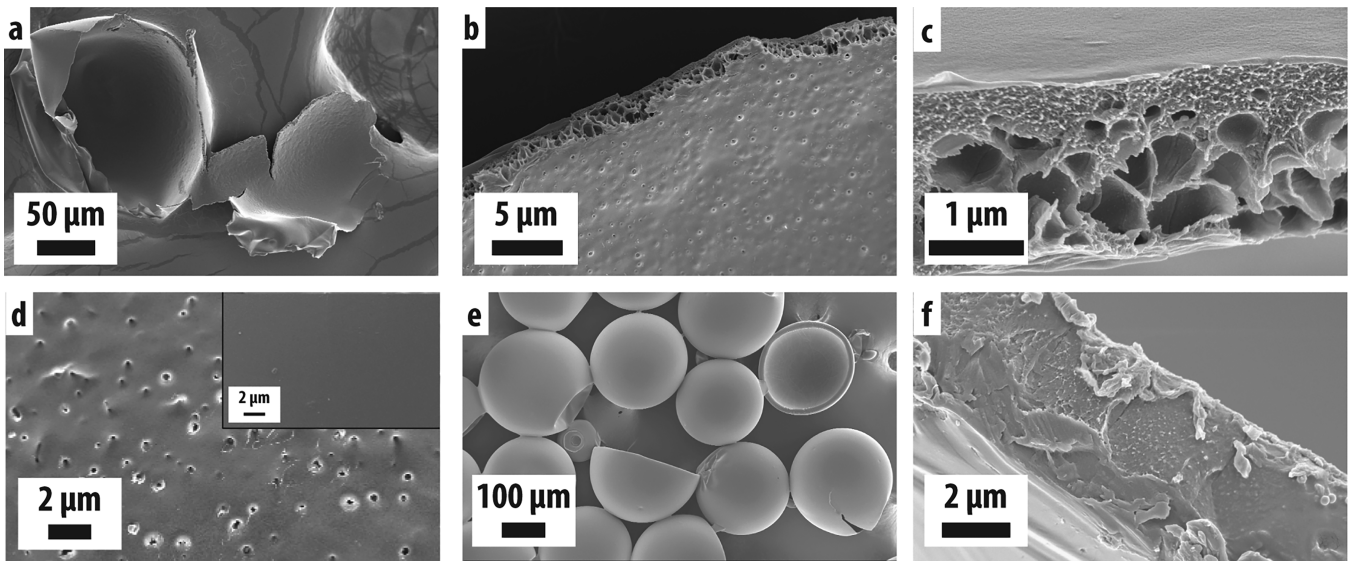

Figure 2. Scanning electron microscopy (SEM) images of (a−d) phase-inverted PMMA microcapsule shells obtained from nonsolvent induced phase separation of double emulsion drops, and (e, f) dense-shell PMMA microcapsules obtained from solvent evaporation without phase inversion. SEM images in (b), (c), and (f) show a cross-section of the PMMA shells, and in (d), the inner surface and the outer surface (inset image) of the phase-inverted shells.

glass capillary microfluidic device is assembled with two tapered cylindrical capillaries from opposite sides within a square capillary, as depicted in Figure 1a. The cylindrical capillary with the smaller tip acts as an inlet for the aqueous core phase and is surface-treated hydrophobically. The second cylindrical capillary acts as the outlet and is rendered hydrophilic. A polymer solution consisting of 6 wt % PMMA in benzyl alcohol (BnOH) and aqueous solutions containing 5 wt % poly(vinyl alcohol) (PVA) and 0.1 wt % hexadecyltrimethylammonium bromide (CTAB) as surfactants are injected into the glass capillary device as middle and inner/outer phases, respectively. All three fluid phases meet between the two tapered orifices where W/O/W double emulsion drops are formed due to the low miscibility of BnOH with water, as shown in Figure 1d. The flow rates are set at 100, 20, and 600 μL/h from inner to outer fluids to form droplets in the dripping mode.[23] The W/O/W double emulsion droplets are collected in a DMSO−water coagulation bath at a volume ratio

https://dx.doi.org/10.1021/acsmacrolett.0c00858
ACS Macro Lett. 2021, 10, 116−121

of 7:3, as depicted in Figure 1a. DMSO serves as a compatibilizer to induce the miscibility between water and BnOH. To illustrate the miscibility of water and BnOH with the presence of DMSO, the ternary phase diagram of the BnOH/DMSO/water system is determined by turbidimetric titration method and shown in Figure 1c. The BnOH−DMSO−water ternary system exhibits areas of miscibility (one-phase region in the white area with circles) and immiscibility (two-phase region in the gray area with crosses) at high and low DMSO content, respectively. When the emulsion drops are immersed into the mixture of water and DMSO, benzyl alcohol diffuses from the shell outward into the coagulation solution, while water and DMSO diffuse into the oil shell from the outer interface. The content of DMSO gradually increases within the oil shell, leading to its composition change with trajectory, indicated by the black arrow in Figure 1c. As the ternary DMSO−water−BnOH system crosses the phase boundary from a two-phase to a single-phase liquid, the solvent of the polymer solution (BnOH) is extracted by the nonsolvent (water). The exchange between BnOH and water causes nonsolvent-induced phase separation (NIPS), where the single-phase homogeneous polymer solution is separated into two phases: a polymer-rich phase and a polymer-lean phase.[24−27] Upon completion of phase inversion, these two phases transform to membrane body and voids, respectively, after solidification, as depicted in Figure 1b. During the immersion process, the continuous water phase is suddenly replaced by DMSO−water solution, causing an osmotic pressure difference between the aqueous core of the capsules and the DMSO−water coagulation bath. After coagulation, the phase-inverted microcapsules are washed with deionized water. The fabrication process yields nonspherical microcapsules, some of which are buckled, but no shell rupture or capsule breakage is observed, as shown in Figure 1e.

During the process of coagulation, the radially outward dissipation of benzyl alcohol on the outer surface of the capsules induces a gradient in polymer concentration along the shell normal with the highest concentration on its outside. The concentration gradient results in an increasing pore size from the outside in, as shown in the scanning electron microscopy images of Figure 2a,b. The cross-section of the phase-inverted PMMA microcapsules exhibit an interconnected, graded macroporous structure. The pore size increases along the shell normal toward the core of the microcapsule, with pore diameters in the 100s of nm close to the outer surface, increasing to micron-sized pores toward the core interface. The outer surface of the microcapsules exhibits a dense skin layer of polymer that serves as the mass transport controlling permeation layer, while the interface between polymer shell and aqueous core contains larger macropores, as shown in Figure 2c,d. To compare the shell structure to flat phase inversion membranes, PMMA NIPS membranes are also cast from benzyl alcohol solution on a solid substrate and phase inverted in a DMSO−water coagulation bath. The obtained phase-inverted PMMA membranes from 10 and 15 wt % solutions exhibit similar graded macroporous structures as the microcapsule shells, with a dense skin layer on the top surface, as shown in Figure S1 (Supporting Information). To evaluate the tunability of the shell structure, phase-inverted microcapsules are fabricated with various inner/middle flow rate ratios ranging from 1:2 to 2:1 and phase-inverted in the coagulation bath with varying DMSO/water ratios. As the inner/middle flow rate ratio increases, phase-inverted microcapsules with a thicker shell are obtained. Phase inversion of double emulsion drops with a core/shell ratio of 1:2 lead to asymmetric shell membranes with a significantly thicker shell and an increased fraction of the dense layer across the shell membrane, as shown in Figure S4a,d,g (Supporting Information). Phase inversion of double emulsion drops with a core/shell ratio of 1:1 and below do not exhibit significant differences in shell thickness and microstructure. Furthermore, varying the DMSO/water ratio in the coagulation bath does not significantly alter the shell microstructure, as shown in Figure S4 (Supporting Information).

To assess the permeability of the microcapsules obtained from phase inversion, the permeation of fluorescent probe molecules of different sizes in water is measured using time-resolved laser-scanning fluorescent confocal microscopy (LSFC). The water-cored microcapsules are challenged with sulforhodamine B (0.559 kg mol^{-1}) and fluorescein-labeled dextran (FITC-dextran, 250 kg mol^{-1}) from the continuous aqueous phase. The permeation of sulforhodamine B into the NIPS PMMA microcapsules takes about 20 min until saturation; this is an order of magnitude faster than for the FITC-dextran, which requires hundreds of minutes to reach saturation, as shown in the evolution of the normalized fluorescence intensity in the cores of the phase-inverted PMMA microcapsules plotted in Figure 3a and corresponding fluorescence micrographs in Figures 3c,d and S2a,b. The difference in time to saturation demonstrates the molecular-size dependence of the permeability of the shells of the phase-inverted microcapsules. We see no evidence of holes or cracks in the capsule shells, which would lead to very rapid transport

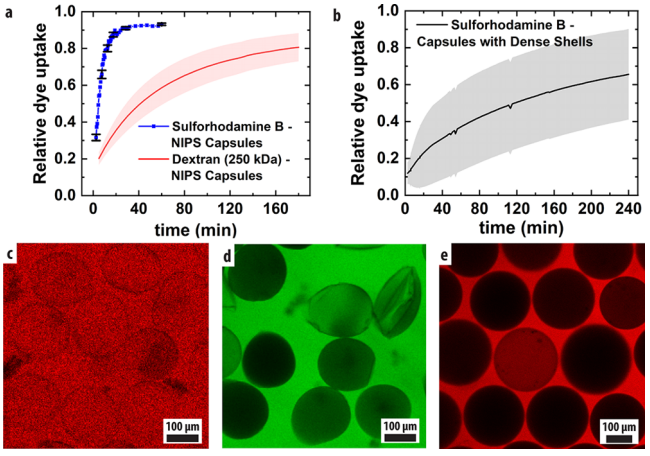

Figure 3. Molecular permeation into PMMA microcapsules. (a) Uptake of sulforhodamine B (blue curve) and FITC-dextran (250 kg mol^{-1}, red curve) into phase-inverted PMMA microcapsules. (b) Uptake of sulforhodamine B into PMMA microcapsules with dense shells obtained from solvent evaporation. The plotted values are the average intensity ratios of the interior to exterior fluorescence of at least 30 capsules and the corresponding vertical width of the shaded region represents the distribution of the permeabilities of the capsules. The vertical width of the shaded region is based on the standard deviation of the normalized fluorescence intensity in the cores of the analyzed microcapsules; the error bars in (a) are based on the standard error of the mean (s.e.m.) of the analyzed capsules. (c−e) LSFC microscopy images of (c, d) phase-inverted and (e) dense-shell PMMA microcapsules 20 min after challenging with (d) FITC-dextran (250 kg mol^{-1}) and (c, e) sulforhodamine B from the exterior of the capsules.

https://dx.doi.org/10.1021/acsmacrolett.0c00858
ACS Macro Lett. 2021, 10, 116−121

of the dye into the core; this demonstrates that the phase-inverted microcapsules survive the shock of osmosis pressure in the coagulation process. The time-dependent permeation of the FITC-dextran into each phase-inverted microcapsule can be measured with sufficient precision to determine the distribution of the permeabilities of the capsules, which is represented by the vertical width of the shaded region of the curve on the right in Figure 3a. By contrast, the time-dependent measurement of the permeation of sulforhodamine B into the phase-inverted capsules is not precise, as indicated by the highly fluctuating curve in Figure S3a. Thus, we show the uncertainty in the mean values of the relative dye uptake by the error bars, which are based on the standard error of the mean (s.e.m.) of the analyzed capsules in Figure 3a.

As a control, the permeation of sulforhodamine B into PMMA microcapsules with dense shells is characterized. The dense-shell capsules are obtained from the solvent evaporation process of double emulsions without phase inversion (Figure 2e,f). When no coagulation bath is employed after the formation of double emulsion drops, benzyl alcohol dissipates slowly through the continuous water phase and evaporates from the water−air interface. The slow dissipation of benzyl alcohol, in the absence of any compatibilizer, results in solidification of the shell through homogeneous drying. The permeation of sulforhodamine B into the resultant dense-shell PMMA microcapsules is much slower than that into the phase-inverted counterparts, as can be seen by comparing the behavior of the dense-shell microcapsules, as shown in Figure 3b, with that of the NIPS capsules shown by the leftmost data in Figure 3a. While the interior of the phase-inverted microcapsules is fully equilibrated with the fluorescence outside of the capsule within 20 min, the dense-shell PMMA microcapsules show almost no uptake of the fluorescent probe molecule over the same time. The much higher permeability of the phase-inverted PMMA microcapsule membranes is attributed to the very thin, dense skin layer, with a thickness of ∼500 nm, an order of magnitude thinner than the thickness of the fully dense-shell PMMA microcapsule membranes, which is approximately 5 μm. While the overall shell thickness of the phase-inverted PMMA microcapsules is also of the order of microns, only the dense skin layer acts as the permeation barrier for separation, whereas rapid permeation occurs through the graded macroporous substructure. The separation process in the dense skin layer is the rate-determining step for permeation in NIPS membranes. Therefore, the overall permeability of the phase-inverted PMMA microcapsules approximates that of ultrathin shell microcapsules, but with enhanced structural stability.

The distribution of the permeabilities of the capsules with dense shells is determined by monitoring the permeation of sulforhodamine B from the exterior into the core of each capsule, as shown in Figure S3c. The distribution of the capsules with dense shells is wide, as indicated by the large vertical width of the shaded region in Figure 3b and shown in LSFC micrographs of Figure S2c. Some dense-shell PMMA microcapsules are impermeable to sulforhodamine B, with no detectable fluorescence inside the core, even after 24 h, whereas others are fully equilibrated with their surrounding within 100 min, as shown in Figure S2c.

To qualitatively assess the structural stability of the microcapsules obtained from phase inversion, an osmotic shock is applied to trigger the mechanical deformation of the phase-inverted microcapsules. The phase-inverted microcapsules are challenged with polyethylene glycol with a molecular weight of 6000 g mol^{-1} (PEG-6000, 0.1 mol L^{-1}) from the exterior aqueous phase. Immediate buckling of the spherical shells of the phase-inverted microcapsules is observed due to the high osmolarity (∼10 MPa) of PEG-6000 solution, as shown in Figure 4a−c. When the high osmotic pressure is removed by diluting the PEG-6000 solution with excess deionized water, the shells of the phase-inverted microcapsules unbuckle slowly and recover a spherical shape, as shown in Figure 4d−f. The buckling and recovery to a spherical shape demonstrates that the phase-inverted PMMA microcapsule membranes are mechanically robust and can undergo osmotically induced shape changes without shell rupture or breakage, an otherwise often-encountered issue with microcapsules.[28−30]

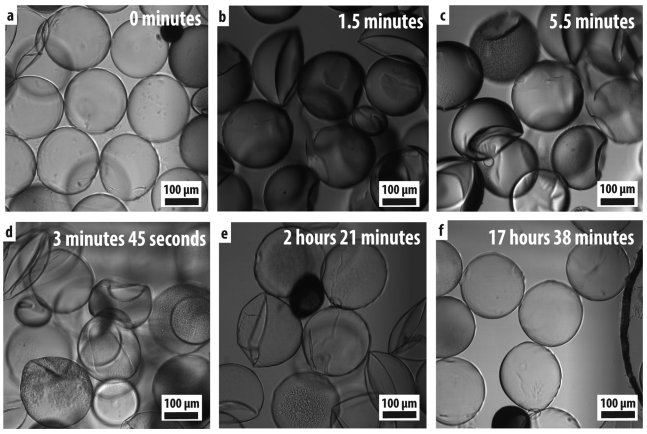

Figure 4. Buckling and unbuckling behavior of the phase-inverted microcapsules. (a) Brightfield laser scanning confocal (LSC) microscopy images of phase-inverted microcapsules in deionized water before the osmotic shock. (b, c) Brightfield LSC microscopy images of phase-inverted microcapsules (b) 1.5 and (c) 5.5 min after challenging with PEG-6000 (0.1 mol L^{-1}) solution. (d−f) LSC microscopy images of phase-inverted microcapsules (d) 3 min 45 s, (e) 2 h 21 min, and (f) 17 h 38 min after the replacement of the exterior PEG-6000 (0.1 mol L^{-1}) solution with deionized water.

In conclusion, we apply phase inversion to double emulsion drop templating to fabricate asymmetric membranes as microcapsule shells. By combining a drop-based microfluidics method with a phase-inversion technique and introducing a compatibilizer in the coagulation bath to induce miscibility between water and the polymer solvent, phase separation within the oil shell of W/O/W double emulsion templated microdroplets is induced. The phase separation leads to the formation of a tailored shell membrane architecture consisting of an ultrathin size-selective separation layer covering a graded macroporous support structure. The formation of such an asymmetric architecture enables high permeability across the capsule shell with molecular selectivity while maintaining structural stability of the shell membrane. The high permeability and well-defined selectivity combined with the structural stability of the phase-inverted microcapsules will increase the potential utility of these capsules. For example, catalysts can be encapsulated in these capsules to facilitate the chemical reactions while being protected from deactivation by the external contaminants. Similarly, the asymmetrically structured morphology produced through the use of phase separation during preparation will enable a broader range of capsule architectures.

https://dx.doi.org/10.1021/acsmacrolett.0c00858
ACS Macro Lett. 2021, 10, 116−121

Poly(methyl methacrylate) (PMMA, M_w = 120 kg mol^{-1}), benzyl alcohol (BnOH, ACS reagent, 99.0%), poly(vinyl alcohol) (PVA, M_w = 13000−23000 g mol^{-1}, 87−89% hydrolyzed), dimethyl sulfoxide (DMSO), hexadecyltrimethylammonium bromide (CTAB), trimethoxy(octadecyl)silane (ODTS, hydrophilic silane), and polyethylene glycol 6000 (PEG-6000, M_w = 5000−7000 g mol^{-1}) are purchased from Sigma-Aldrich and used as received. 2-[Methoxy-(polyethyleneoxy)6-9propyl] trimethoxysilane (tech-90) are purchased from Gelest and used as received.

The phase diagram of the BnOH−DMSO−water ternary system is determined by quantitative addition of DMSO to mixtures of BnOH/water with different ratios. The BnOH/water solutions are vigorously mixed by a vortex mixer each time after the addition of an aliquot of DMSO and inspected visually until the mixtures turn from the turbid two-phase state into a transparent homogeneous phase. Compositions corresponding to the volume fractions of the pure liquids added to the mixture are plotted in Figure 1c.

W/O/W double emulsion drops are generated in a glass capillary microfluidic drop makers,[20] as described previously. The interior of the glass capillary device is first flushed with outer phase (5 wt % PVA and 0.1 wt % CTAB in water) to avoid precipitation of the PMMA polymer during the drop-making process. The inner (5 wt % PVA and 0.1 wt % CTAB in water), middle (6 wt % PMMA in BnOH), and outer (5 wt % PVA and 0.1 wt % CTAB in water) phases are injected into the small-tipped cylindrical capillary, the interstitial space of the small-tipped cylindrical and the square capillary, and the interstitial space of the large-tipped cylindrical and the square capillary, respectively. The flow rate of each phase is adjusted to form double emulsion drops in the dripping mode. Droplet formation is recorded with a Phantom V9.0 high-speed camera connected to the inverted microscope. The W/O/W double emulsion microdroplets are collected into a vial containing excess DMSO and water at a volume ratio of 7:3 for coagulation. For the fabrication of PMMA microcapsules with dense shells, the double emulsion drops are collected in a vial containing excess aqueous outer phase and left in an open atmosphere for 24 h for solvent evaporation and homogeneous shell solidification.

The microcapsules are washed three times with deionized water to remove residuals of PVA, CTAB, and DMSO. The structure of the microcapsule shells is determined by scanning electron microscopy (SEM). Samples are prepared by depositing an aqueous dispersion of capsules on double-sided carbon adhesive conductive carbon tape on aluminum SEM specimen holders and subsequently dried in air. Some of the capsules are sectioned by a razor blade under an optical microscope after drying to view the cross-section and inner structures of the microcapsules. The SEM samples are sputter-coated (EMS 300T D Dual Head Sputter Coater) with a conductive layer of Pt/Pd 80/20 prior to imaging. The shell morphology of the microcapsules is observed on a Zeiss Ultra Plus FESEM equipped with an in-lens detector at an acceleration voltage of 3 kV.

Permeation into the microcapsules is characterized with sulforhodamine B (0.559 kg mol^{-1}) and FITC-dextran (250 kg mol^{-1}) as fluorescent probe molecules. Stock solutions of dye are prepared at a concentration of 0.1 mg mL^{-1} for the sulforhodamine B and 1 mg mL^{-1} for the FITC-dextran. To test the size-dependent permeability of the capsules, an 80 μL sample of as-prepared microcapsules are loaded into a well and is challenged with 20 μL of stock solution of a specific dye. Fluorescent signal intensity in and around the capsules is captured with LSFC microscopy (Leica SP-5) at a fixed time interval since the addition of fluorescent molecular dye solution. For detection of FITC-dextran, the excitation wavelength is 488 nm and the detector wavelength range is 490−540 nm, whereas for detection of sulforhodamine B, the excitation wavelength is 543 nm and the detector wavelength range is 600−650 nm. The confocal images are analyzed with ImageJ to obtain the average fluorescence intensity in the cores of the microcapsules. The average core intensity is divided by the concurrent outside intensity of the capsules to obtain a normalized "dye uptake" value.

Mechanical stability of the phase-inverted microcapsules is qualitatively assessed by applying osmotic pressure to the capsules. The phase-inverted microcapsules are washed three times with deionized water, loaded into a well, and challenged with an aqueous solution of PEG-6000. The PEG-6000 solution is subsequently diluted with excess deionized water. The corresponding buckling and unbuckling behavior of the phase-inverted microcapsules is recorded with LSC microscopy (Leica SP-5).

■ ASSOCIATED CONTENT

Supporting Information

The Supporting Information is available free of charge at https://pubs.acs.org/doi/10.1021/acsmacrolett.0c00858.

Scheme of flat phase-inversion membrane fabrication procedure and structures characterized by SEM, confocal images captured during dye permeation test of microcapsules, details on materials and solutions, experimental methods for measuring ternary phase diagram, fabrication of flat membranes and NIPS microcapsules, characterization of microcapsules with SEM, and dye permeation test on microcapsules (PDF)

■ AUTHOR INFORMATION

Corresponding Authors

Jörg G. Werner − *John A. Paulson School of Engineering and Applied Sciences, Harvard University, Cambridge, Massachusetts 02138, United States; Department of Mechanical Engineering and Division of Materials Science and Engineering, Boston University, Boston, Massachusetts 02215, United States;* orcid.org/0000-0001-7845-086X; Email: jgwerner@bu.edu

David A. Weitz − *John A. Paulson School of Engineering and Applied Sciences, Harvard University, Cambridge, Massachusetts 02138, United States; Department of Physics, Harvard University, Cambridge, Massachusetts 02138, United States;* orcid.org/0000-0001-6678-5208; Email: weitz@seas.harvard.edu

Author

Zhang Wu − *John A. Paulson School of Engineering and Applied Sciences, Harvard University, Cambridge, Massachusetts 02138, United States;* orcid.org/0000-0003-0569-7014

Complete contact information is available at: https://pubs.acs.org/10.1021/acsmacrolett.0c00858

https://dx.doi.org/10.1021/acsmacrolett.0c00858
ACS Macro Lett. 2021, 10, 116−121

Author Contributions

The manuscript was written through contributions of all authors. All authors have given approval to the final version of the manuscript.

Notes

The authors declare no competing financial interest.

■ ACKNOWLEDGMENTS

This work was supported by the National Science Foundation (DMR-1708729) and National Science Foundation through the Harvard University MRSEC (DMR-1420570). This work was performed in part at the Center for Nanoscale Systems (CNS), a member of the National Nanotechnology Coordinated Infrastructure Network (NNCI), which was supported by the National Science Foundation under NSF Award No. 1541959. CNS is part of Harvard University.

■ REFERENCES

(1) Kim, J. H.; Jeon, T. Y.; Choi, T. M.; Shim, T. S.; Kim, S. H.; Yang, S. M. Droplet Microfluidics for Producing Functional Microparticles. *Langmuir* **2014**, *30*, 1473−1488.
(2) Li, W.; Zhang, L.; Ge, X.; Xu, B.; Zhang, W.; Qu, L.; Choi, C. H.; Xu, J.; Zhang, A.; Lee, H.; Weitz, D. A. Microfluidic Fabrication of Microparticles for Biomedical Applications. *Chem. Soc. Rev.* **2018**, *47*, 5646−5683.
(3) Dittrich, P. S.; Manz, A. Lab-on-a-Chip: Microfluidics in Drug Discovery. *Nat. Rev. Drug Discovery* **2006**, *5*, 210−218.
(4) LaVan, D. A.; McGuire, T.; Langer, R. Small-Scale Systems for in Vivo Drug Delivery. *Nat. Biotechnol.* **2003**, *21*, 1184−1191.
(5) Samanta, B.; Yang, X. C.; Ofir, Y.; Park, M. H.; Patra, D.; Agasti, S. S.; Miranda, O. R.; Mo, Z. H.; Rotello, V. M. Catalytic Microcapsules Assembled from Enzyme-Nanoparticle Conjugates at Oil-Water Interfaces. *Angew. Chem., Int. Ed.* **2009**, *48*, 5341−5344.
(6) Liu, D.; Herranz-Blanco, B.; Mäkilä, E.; Arriaga, L. R.; Mirza, S.; Weitz, D. A.; Sandler, N.; Salonen, J.; Hirvonen, J.; Santos, H. A. Microfluidic Templated Mesoporous Silicon-Solid Lipid Microcomposites for Sustained Drug Delivery. *ACS Appl. Mater. Interfaces* **2013**, *5*, 12127−12134.
(7) Loiseau, E.; Niedermair, F.; Albrecht, G.; Frey, M.; Hauser, A.; Rühs, P. A.; Studart, A. R. Strong Microcapsules with Permeable Porous Shells Made through Phase Separation in Double Emulsions. *Langmuir* **2017**, *33*, 2402−2410.
(8) Chen, P. W.; Erb, R. M.; Studart, A. R. Designer Polymer-Based Microcapsules Made Using Microfluidics. *Langmuir* **2012**, *28*, 144−152.
(9) Chen, P. W.; Brignoli, J.; Studart, A. R. Mechanics of Thick-Shell Microcapsules Made by Microfluidics. *Polymer* **2014**, *55*, 6837−6843.
(10) Zhang, M. J.; Wang, W.; Yang, X. L.; Ma, B.; Liu, Y. M.; Xie, R.; Ju, X. J.; Liu, Z.; Chu, L. Y. Uniform Microparticles with Controllable Highly Interconnected Hierarchical Porous Structures. *ACS Appl. Mater. Interfaces* **2015**, *7*, 13758−13767.
(11) Wang, B.; Prinsen, P.; Wang, H.; Bai, Z.; Wang, H.; Luque, R.; Xuan, J. Macroporous Materials: Microfluidic Fabrication, Functionalization and Applications. *Chem. Soc. Rev.* **2017**, *46*, 855−914.
(12) Dinsmore, A. D.; Hsu, M. F.; Nikolaides, M. G.; Marquez, M.; Bausch, A. R.; Weitz, D. A. Colloidosomes: Selectively Permeable Capsules Composed of Colloidal Particles. *Science* **2002**, *298*, 1006−1009.
(13) Tipnis, R.; Vaddiraju, S.; Jain, F.; Burgess, D. J.; Papadimitrakopoulos, F. Layer-by-Layer Assembled Semipermeable Membrane for Amperometric Glucose Sensors. *J. Diabetes Sci. Technol.* **2007**, *1*, 193−200.
(14) Lee, D.; Weitz, D. A. Double Emulsion-Templated Nanoparticle Colloidosomes with Selective Permeability. *Adv. Mater.* **2008**, *20*, 3498−3503.
(15) Kim, B.; Lee, T. Y.; Abbaspourrad, A.; Kim, S. H. Perforated Microcapsules with Selective Permeability Created by Confined Phase Separation of Polymer Blends. *Chem. Mater.* **2014**, *26*, 7166−7171.
(16) Tong, W.; Song, X.; Gao, C. Layer-by-Layer Assembly of Microcapsules and Their Biomedical Applications. *Chem. Soc. Rev.* **2012**, *41*, 6103−6124.
(17) Tong, W.; Gao, C. Multilayer Microcapsules with Tailored Structures for Bio-Related Applications. *J. Mater. Chem.* **2008**, *18*, 3799−3812.
(18) Johnston, A. P. R.; Cortez, C.; Angelatos, A. S.; Caruso, F. Layer-by-Layer Engineered Capsules and Their Applications. *Curr. Opin. Colloid Interface Sci.* **2006**, *11*, 203−209.
(19) Murua, A.; Portero, A.; Orive, G.; Hernández, R. M.; de Castro, M.; Pedraz, J. L. Cell Microencapsulation Technology: Towards Clinical Application. *J. Controlled Release* **2008**, *132*, 76−83.
(20) Utada, A. S.; Lorenceau, E.; Link, D. R.; Kaplan, P. D.; Stone, H. A.; Weitz, D. A. Monodisperse Double Emulsions Generated from a Microcapillary Device. *Science* **2005**, *308*, 537−541.
(21) Datta, S. S.; Abbaspourrad, A.; Amstad, E.; Fan, J.; Kim, S. H.; Romanowsky, M.; Shum, H. C.; Sun, B.; Utada, A. S.; Windbergs, M.; Zhou, S.; Weitz, D. A. 25th Anniversary Article: Double Emulsion Templated Solid Microcapsules: Mechanics and Controlled Release. *Adv. Mater.* **2014**, *26*, 2205−2218.
(22) Shah, R. K.; Shum, H. C.; Rowat, A. C.; Lee, D.; Agresti, J. J.; Utada, A. S.; Chu, L. Y.; Kim, J. W.; Fernandez-Nieves, A.; Martinez, C. J.; Weitz, D. A. Designer Emulsions Using Microfluidics. *Mater. Today* **2008**, *11*, 18−27.
(23) Nunes, J. K.; Tsai, S. S. H.; Wan, J.; Stone, H. A. Dripping and Jetting in Microfluidic Multiphase Flows Applied to Particle and Fiber Synthesis. *J. Phys. D: Appl. Phys.* **2013**, *46*, 114002.
(24) Loeb, S.; Sourirajan, S. In *Saline Water Conversion II*; Gould, R. F., Ed.; American Chemical Society: Washington, DC, 1963; Vol. *38*, p 117.
(25) Kesting, R. E. In *Materials Science of Synthetic Membranes*; Lloyd, D. R., Ed.; American Chemical Society: Washington, DC, 1985; Vol. *269*, p 131.
(26) Guillen, G. R.; Pan, Y.; Li, M.; Hoek, E. M. V. Preparation and Characterization of Membranes Formed by Nonsolvent Induced Phase Separation: A Review. *Ind. Eng. Chem. Res.* **2011**, *50*, 3798−3817.
(27) Hołda, A. K.; Vankelecom, I. F. J. Understanding and Guiding the Phase Inversion Process for Synthesis of Solvent Resistant Nanofiltration Membranes. *J. Appl. Polym. Sci.* **2015**, *132*, 42130.
(28) Abbaspourrad, A.; Carroll, N. J.; Kim, S.-H.; Weitz, D. A. Polymer Microcapsules with Programmable Active Release. *J. Am. Chem. Soc.* **2013**, *135*, 7744−7750.
(29) Zhang, W.; Qu, L.; Pei, H.; Qin, Z.; Didier, J.; Wu, Z.; Bobe, F.; Ingber, D. E.; Weitz, D. A. Controllable Fabrication of Inhomogeneous Microcapsules for Triggered Release by Osmotic Pressure. *Small* **2019**, *15*, 1903087.
(30) Zhang, W.; Abbaspourrad, A.; Chen, D.; Campbell, E.; Zhao, H.; Li, Y.; Li, Q.; Weitz, D. A. Osmotic Pressure Triggered Rapid Release of Encapsulated Enzymes with Enhanced Activity. *Adv. Funct. Mater.* **2017**, *27*, 1700975.

https://dx.doi.org/10.1021/acsmacrolett.0c00858
ACS Macro Lett. 2021, 10, 116−121